Microelectronics Reliability 51 (2011) 931–935

Contents lists available at ScienceDirect

Microelectronics Reliability

journal homepage: www.elsevier.com/locate/microrel

Luminescence properties of mechanically nanoindented ZnSe

Wei-Hung Yau [a], Pai-Chung Tseng [a], Hua-Chiang Wen [b,d,*], Chien-Huang Tsai [c], Wu-Ching Chou [d]

[a] Department of Mechanical Engineering, National Chung Hsing University, Taichung 40227, Taiwan, ROC
[b] Department of Material Engineering, National Chung Hsing University, Taichung 40227, Taiwan, ROC
[c] Department of Automation Engineering, Nan Kai University of Technology, Nantou 54243, Taiwan, ROC
[d] Department of Electrophysics, National Chiao Tung University, Hsinchu 300, Taiwan, ROC

ARTICLE INFO

Article history:
Received 24 February 2010
Received in revised form 10 January 2011
Accepted 10 January 2011
Available online 17 February 2011

ABSTRACT

In this study, we used cathodoluminescence (CL) spectroscopy to examine the CL emissions of zinc selenide (ZnSe) single crystals that had been subjected to Berkovich nanoindentation. The CL spectra of the ZnSe exhibited both impurity emission peaks (1.8–2.4 eV band) and near-bandgap emission peaks (2.68 eV). Although CL emissions were generated during four unloading/reloading cycles, the decreased intensity of the impurity emission can be explained in terms of extended dislocation nucleation and propagation during nanoindentation. The resultant dislocation and microcracks were visualized using CL mapping and transmission electron microscopy. We suspect that the formation of a hysteresis loop during the four unloading/reloading cycles was due, in part, to massive dislocation activities induced by the indenter.

1. Introduction

Zinc selenide (ZnSe) is one of the most attractive group II–VI semiconductors because of its outstanding potential for the development of optoelectronic devices. ZnSe materials exhibit several favorable optoelectronic characteristics including emission/absorption signals ranging from the ultraviolet to the infrared, a wide bandgap, and low resistivity that make them ideally suitable for preparing high-efficiency photodiodes that operate in the UV–Vis range. ZnSe compounds are used in commercialized thin film electroluminescence displays that are produced using either sputtering or chemical deposition methods [1–7].

Because II–VI semiconductor materials feature weak atomic bonds and readily generate defects, they often exhibit poor mechanical performance. Indeed, device lifetimes are limited to well below practical levels because of defect generation and propagation during operation [8]. In mobile systems, mechanical loads can arise from shock loading during fabrication and handling processes, leading to mechanical damage of their desired characteristics. The advent of nanoindentation instruments has led to greater understanding of the underlying principles that affect contact loading and related phenomena. Nanometer-scale nanoindentation has been used widely to investigate the deformation mechanisms of various semiconductors [9,10]. The mechanical characteristics of solid surfaces, such as hardness and Young's modulus, can be extracted from such studies [11–13].

Studies of microstructures are important not only for the development of viable devices but also because they efficiently provide data regarding photoelectric properties. That is, if we are to integrate ZnSe into a device, we require a good understanding of its mechanical characteristics [14] to enhance the reliability of the device. Grillo et al. [15] found that the hardness of ZeSe was anisotropic, depending on the orientation of the side of the Berkovich pyramid relative to the [1 0 0] direction. This information is important when growing ZnSe films on Si substrates. Grillo et al. [15] also noted, from a nanoindentation study using a Berkovich-type indenter, that the alloying of ZnSe with a more-covalent II–VI compound, such as BeSe (forming $Zn_{1-x}Be_xSe$ heteroepitaxial layers), can significantly alter its mechanical properties; no attempts have been made, however, to use the nanoindentation method to investigate the deformation-induced crystal defects or hysteresis loops of ZnSe.

In this study, we used cathodoluminescence (CL) in scanning electron microscopy (SEM) and transmission electron microscopy (TEM) to investigate the Berkovich-induced deformation of ZnSe by means of nanoindentation instruments. Herein, we describe the changes in ZnSe CL spectra and our observations of dark slip lines.

2. Experimental Details

Single-crystal ZnSe was obtained through solid phase recrystallization and polished mechano-chemically using standard procedures. The (1 0 0)-oriented ZnSe substrates were cut from crystals grown by solid phase recrystallization; the details of the growth procedures used to prepare the single crystals of ZnSe have

* Corresponding author at: Department of Electrophysics, National Chiao Tung University, Hsinchu 300, Taiwan, ROC. Tel.: +886 (4) 22840500x409; fax: +886 (4) 22854563.
E-mail address: a091316104@gmail.com (H.-C. Wen).

0026-2714/$ - see front matter © 2011 Elsevier Ltd. All rights reserved.
doi:10.1016/j.microrel.2011.01.005

been described previously [16]. To investigate the mechanical behavior, nanoindentation measurements were performed using a Nanoindenter MTS NanoXP system (MTS Corporation, Nano Instruments Innovation Center, TN, USA) equipped with a diamond pyramid-shaped Berkovich-type indenter tip (radius of curvature: 50 nm); stiffness data were recorded along with the load and displacement curve. The hardness and Young's modulus of ZnSe were calculated from the load–displacement (P–h) data using the analytical method developed by Oliver and Pharr [17]. Each value, reported here together with its standard deviation, resulted from averaging the results of 12 indentations. The thermal drift was maintained below ±0.05 nm/s for all indentations considered herein.

A 12 × 1 indentation array was produced with each indentation being separated by 50 μm. Using this approach, possible interactions between two consecutive indentation tests were minimized. Each indentation was controlled using an indentation load of 200 mN. In each indentation test, the Berkovich diamond indenter was operated with typical and four-cycle nanoindentation P–h curves; the loading/unloading time was held constant at 30 s and the peak load was held for 5 s.

The nanoindentation-induced mechanical deformations of ZnSe were characterized using a CL apparatus (HORIBA Co. Ltd.). Room-temperature CL measurements and CL mapping were performed using a JEOL JSM-7001F field-emission scanning electron microscope. An electron beam energy of 20 keV was selected to excite the ZnSe surface. The CL light was dispersed by a 2400-nm grating spectrometer and detected by a liquid N_2–cooled charge-coupled device. Firstly, CL spectra are recorded from ZnSe samples just in real time at a fixed electron beam energy of 20 keV. In addition, the corresponding CL image from the surface was displayed on video monitors. The CL images were recorded with the total emitted integral (panchromatic) CL as well as with light of a fixed spectral wavelength (550 nm) by using a suitable charge-coupled device (CCD).

The morphologies and microstructures of the samples were determined using field-emission SEM (FESEM) and TEM. For TEM, the lamellae were examined using a JEOL-JEM 2100F transmission electron microscope operated at 200 kV (point-to-point resolution: 0.23 nm; lattice resolution: 0.14 nm). TEM samples were prepared using the lift-out technique and a dual-beam focused ion beam (FIB) station (FEI Nova 220); details of the FIB method have been reported previously [18].

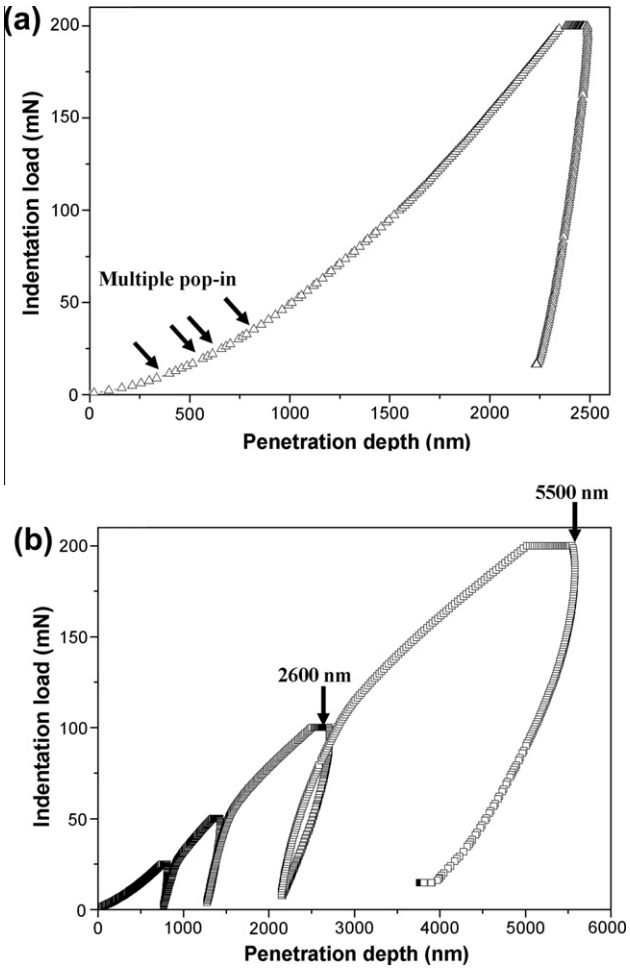

Fig. 1. Load–displacement curves for ZnSe: (a) typical and (b) four unloading/reloading cycles.

3. Results and discussion

Fig. 1 displays typical and four-cycle unloading/reloading P–h curves of ZnSe samples subjected to maximum indentation loads of 200 mN. The measured hardnesses with the typical and four unloading/reloading cycles were 1.4 ± 0.03 and 1.5 ± 0.07 GPa, respectively; the measured Young's moduli were 95.3 ± 1.1 and 192.5 ± 2.3 GPa, respectively. For the typical cycle (Fig. 1a), the irregularities in the P–h curve during the loading process were characterized by slight jumps in the penetration depth-so-called multiple "pop-in" events in the penetration depth. Multiple "pop-in" events are accruable over a wide range of indentation loads and penetration depths, particularly in the plastic deformation of ZnSe samples (arrows in Fig. 1a). Notably, we observed slight multiple "pop-in" events upon increasing the loading up to 100 mN. As expected, these phenomena appeared during the typical cycle, but not during the repeated unloading/reloading cycles (Fig. 1b). The multiple "pop-in" events were evident over a wide range of indentation loads and penetration depths. We suspect that this phenomenon was not thermally activated for repeated unloading/reloading cycles. Multiple "pop-in" events have been reported recently [19] in hexagonally structured materials, including sapphire [20], single-crystal bulk ZnO [21], and GaN [22]. In contrast, single "pop-in" events have been observed in samples having cubic structures, including GaAs and InP [23]. Dislocation-induced "pop-in" events tend to be associated with two distinct deformation behaviors: before (pure elastic behavior) and after (elastoplastic behavior) [24]. From a study of indented ZnSe, Wolf et al. reported [25] that deformation at a high contact pressure was not based on a phase transformation, unlike that of Si and InSb. In Fig. 1b, we observe larger deviations in the penetration depth–indentation load curves for the ZnSe sample subjected to four repeated unloading/reloading cycles; the penetration depth not only suddenly increased from 2600 to 5500 nm (arrows in Fig. 1b) during the last unloading/reloading cycle but also resulted in hysteresis loops. Herein, the higher elastic modulus is the key reason for the appearance of hysteresis loops dependent on the number of nanoindentation cycles. The increases in hardness and Young's moduli during repeated unloading/reloading cycles can be attributed to multistep indentation inducing more plastic deformation relative to single indentation. Wolf et al. suggested [25] that the deformation after the first tip-sample contact is purely elastic. The dislocation-dominated deformation can have more resistance to elastic and plastic deformation [26]. Thus, we observed multiple "pop-in" events in the typical unloading/reloading P–h curves of ZnSe sample. In contrast, it was not easy to observe multiple "pop-in" events in the four-cycle unloading/reloading P–h curves, presumably because the four-cycle unloading/reloading process can relax active dislocation propagation.

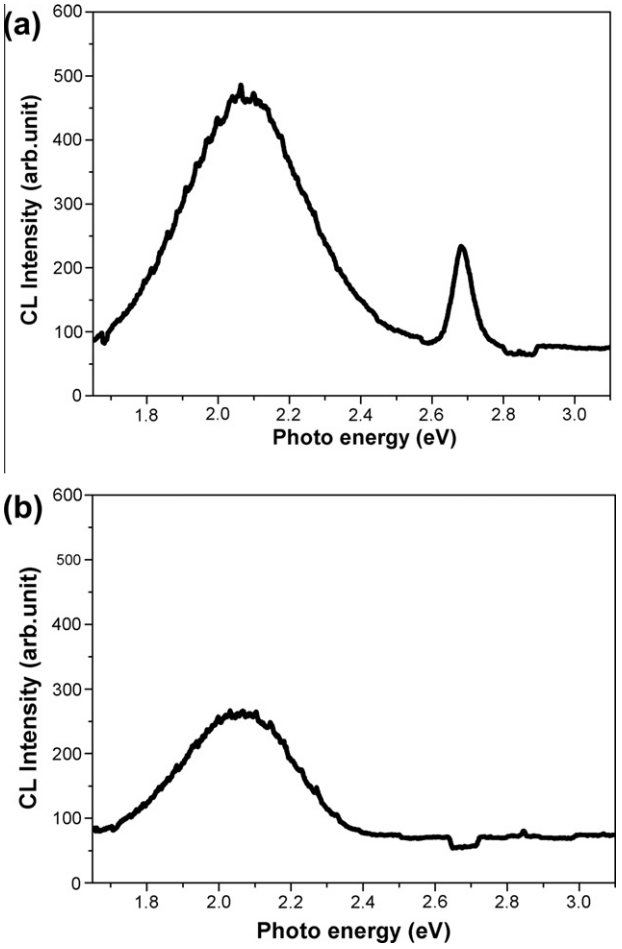

Fig. 2. CL spectra of the ZnSe samples at liquid N_2 temperature: (a) non-indentation and (b) four unloading/reloading cycles.

The main luminescence band in ZnSe appears centered at 2.68 eV. This band is due to the near-bandgap emission, which can be attributed to recombination between electrons bound to Cl donors and free holes in the valence band (Fig. 2a). The very broad emission from 1.8 to 2.4 eV, which dominates the spectrum, can be assigned to Cl impurities, which were partially incorporated into the lattice during the growth process. Near the surface, the long wavelength band at 2.1 eV predominates. Fig. 2b displays the near-bandgap emissions in the CL spectra recorded from ZnSe samples that had been indented using four unloading/reloading cycles. The residual indentations were directly excited using the CL system. With typical loading of the indentation center, the near-bandgap CL emission from ZnSe was dramatically suppressed because of induced defects and/or dislocations. Coleman et al. reported [27] that the CL intensity measured in the bulk is lower than that of a residual indent. Bradby et al. studied [28] the extent of radial propagation of contact-induced defects in ZnO; they observed dramatic suppression of the CL near-bandgap emission from the central regions of the residual indent impressions. In fact, dislocations act as non-radiative recombination centers that quench the luminescence locally. The CL spectrum of the indented area of the ZnSe sample below the level of the critical "pop-in" phenomenon revealed a slight reduction in the intensity of the CL emission, particularly for the very broad emission. Fernandez et al. [14] also noted that irradiation had an effect on the CL spectra, presumably as a result of complex formation or charge transfer processes caused by new point defects (2.0–2.2 eV) as well as higher concentrations of point defects in the deformed samples.

ZnSe possesses either a sphalerite structure, with lattice parameter a of 5.668 Å, or a wurtzite structure, with lattice parameters a and c of 3.820 and 6.626 Å, respectively. The primary slip system of the ZnSe sphalerite structure is $(1\ 1\ 1)\langle 1\ -1\ 0\rangle$, which also consists of five independent systems. Based on strong asymmetry between the dislocation mobilities of the Zn- and Se-terminated dislocations in the active glide-set, the mobility of the Se(g) dislocations is ca. 100 times higher than that of Zn(g) dislocations [25,29,30]. In this case, the hysteresis loops may be based on several

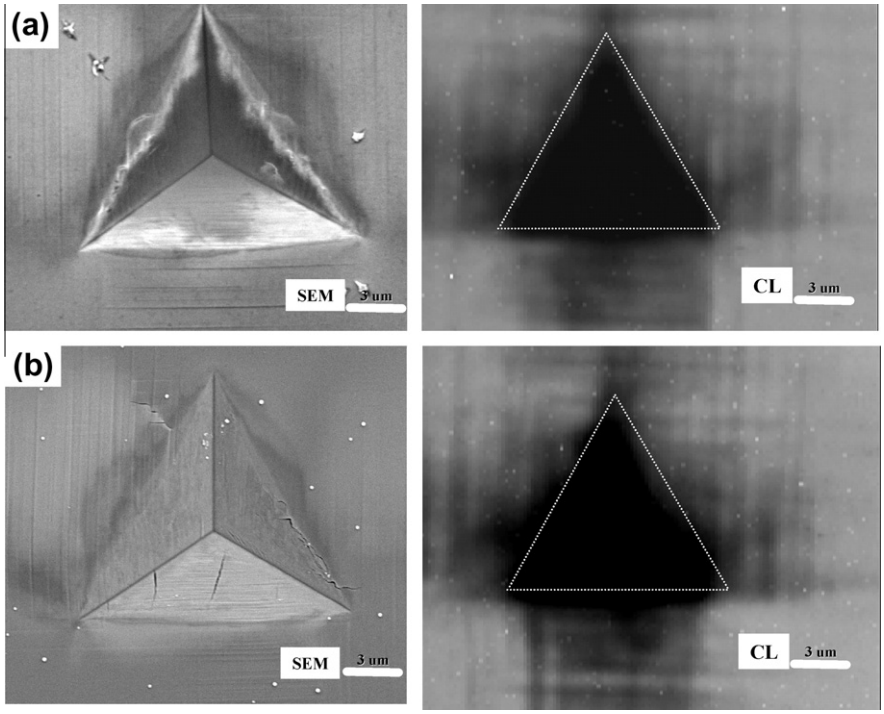

Fig. 3. SEM and CL mapping images of the surface morphologies of ZnSe samples: (a) typical and (b) four unloading/reloading cycles.

unloading/reloading cycles, which cause the ZnSe sample to crack. Again, the primary slip system of ZnSe may play an important role during such testing, where it displayed an enhancement of the very broad CL emission (2.1 eV), greater than that of typical indentation loading (Fig. 2).

SEM images (Fig. 3a) did not provide, for such an indentation load, any evidence of dislocation activity or crack features. They could be observed only when the ZnSe layer was indented under 200 mN, corresponding to a penetration depth of over 5500 nm, where several creeps were observed (Fig. 3b). This behavior leads to larger deviations in the plots of penetration depth with respect to indentation load; similar phenomena have been reported previously [31,32]. Fig. 3 also presents the room-temperature CL images acquired at a bandgap of 2.68 eV from a ZnSe sample indented using a typical cycle and four unloading/reloading cycles to maintain a maximum load of 200 mN. These CL images reveal the distribution of indentation-induced extended defects that alter the CL emission (Fig. 3a). The cube-corner indenter form and these extended defects reflect some of the radial symmetry of the stress field. In contrast, another luminescence/topography distribution CL image revealed a crack line that formed after four unloading/reloading cycles (Fig. 3b). Slip enhancement may contribute to the "crack" observed during unloading/reloading; the mechanism may be due to the plastic deformation of ZnSe [6]. Fernandez et al. [14] reported that the deformed samples that provided total CL intensity decreases possessed dark lines that correspond to slip bands, while the bright lines represent the undeformed background. In this present study, we observed changes in ZnSe CL spectra and dark slip lines (Fig. 3). The indentation mark reveals a strong quenching of the luminescence in the damaged area; at the same time, the surrounding indentation mark displays dark lines corresponding to slip bands. Interestingly, the CL image of the ZnSe indented area below the propagation of dislocations in ZnSe revealed a reduction in the intensity of the CL emission. Coleman et al. [27] suggested that the excitonic emission of ZnO sample is quenched at the indent site. Their analysis of CL monochromatic images and spectra revealed defect states that were responsible for the broad defect emission band. Herein, the cube-corner indenter form and these extended defects reflect some of the radial symmetry of the stress field in the ZnSe sample. We suggest that these extended lines might be indicative of non-radiative defect bands caused by defects extending away from the indent site or by strain-induced migration away from the defect bands.

After the four unloading/reloading cycles, in which only a small percentage of indentations were plastically deformed, CL imaging could distinguish between the indentations that had undergone several degree of plastic deformation (after the "pop-in" event) and indents that were purely in the elastic regime (before the "pop-in" event). As a result, we detected an observable CL impression only after the "pop-in" event, providing convincing evidence that the phenomenon involves the nucleation of a slip as the deformation mode.

Bradby, Kucheyev, and co-workers reported that GaN samples indented under a spherical indenter displayed symmetrical, Star of David–like distributions of defect reflects [20,33]. In addition, Zaldívary et al. [34] reported less symmetrical structures, due to the different distribution of stresses, when using their Vickers indenter. Using the Berkovich-type indenter tip, the CL monochromatic imaging allowed us to distinguish between indentations that had undergone several unloading/reloading cycles during plastic deformation. As a result, we did not observe only a CL impression after the crack-convincing evidence that the unloading/reloading cycles involve a CL emission, especially in the behavior of the dislocation recovery and mobilities. Therefore, in studies of this plastic deformation process, it is essential to delineate the natural role of the material as the indenter penetrates into the surface.

Next, we identified the effects of the deformation mechanisms specific to Berkovich nanoindentation on the microstructures characteristics and CL emissions in the vicinity of the indented area. The cross-sectional TEM image of ZnSe after indentation reveals (Fig. 4a) that the fracture behavior underneath the indented spot was initially a dislocation activity. That is, some dislocations tended to follow directions of easy slip, and may be pinned between slip bands [34]. The slip bands (dark thick lines in the TEM image) clearly reveal that, during indentation, the rapidly produced dislocations could slip partially along the easy-slip directions. We suspect that the highly strained features nearby the indented interface were not just accidental artifacts that resulted from the bare sample. Thus, during the unloading/reloading cycle, the further propagation of indentation-produced dislocations will be impeded. In this case, further plastic deformation must involve the nucleation of additional slip bands, resulting in multiple "pop-in" events, as observed experimentally in Fig. 1.

The TEM images reveal serious cracking while the indentation was made; the molecular bonds were also influenced by the dislocation propagation. Fig. 4b displays a typical microstructure of a heavily deformed material, characterized by features having a high density of dislocations. The distorted slip bands and the extremely high dislocation densities at the intersections indicate a highly

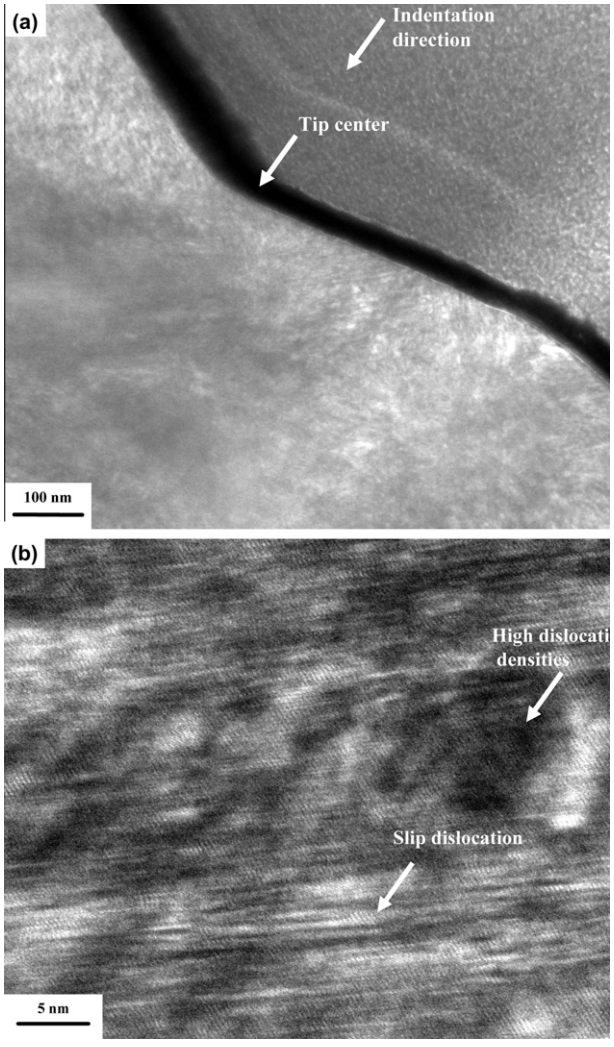

Fig. 4. Cross-sectional TEM images of a ZnSe sample subjected to four unloading/reloading cycles: (a) indented within interfacial view and (b) indented within high-resolution image.

strained state of ZnSe. Nevertheless, even on the submicron scale, we observed no evidence of subsurface cracking or film fragmentation. Thus, the primary deformation mechanism for ZnSe is dislocation nucleation and propagation along easy-slip systems. The mechanism in the dislocation recovery appears to be associated with the activation of dislocation sources during the unloading/reloading cycles of the ZnSe. The plastic deformation that occurred prior to performing the unloading/reloading cycles was associated with the individual movement of a small number of newly nucleated, large shear stresses that quickly accumulated underneath the indenter tip; rapid recovery occurred during the unloading/reloading cycles (Fig. 2). When the local stress underneath the tip was reached after a higher number of cycles, a burst of collective dislocation movement on the easy-slip systems was activated, resulting in a large release of local stress. Each of these collective dislocation movements is reflected as a slip band in the indented microstructure displayed in Fig. 4. Although slip bands appeared in the ZnSe sample in Fig. 1b, the released stress due to this effect could extend deep into the ZnSe. The narrow spacing of dense bands of defects and/or dislocations along the basal planes near the ZnSe surface suggests that, during the later stages of the four unloading/reloading cycles, a large applied indentation load (e.g., 200 mN) began to activate extensive slip bands along the ca. 60° pyramidal planes, thereby resulting in CL emission (Fig. 2b). Therefore, from the TEM observations, the extensive interactions between the dislocations slipping along the ZnSe surface confined the slip bands and resulted in hysteresis loops, due to the heavily deformed and strain-hardened lattice structure. To obtain a closer look at the dislocation activities immediately beneath the Berkovich indenter tip, herein, we obtained a more detailed image of the microstructures (TEM, CL mapping) near the intersections of the slip bands.

4. Conclusion

Using a combination of nanoindentation, CL, and TEM techniques, we have investigated the contact-induced structural deformation behavior of single-crystal ZnSe. These measurements revealed both the surface mechanical properties and the luminescent characteristics of ZnSe. The nanoindentation-induced mechanical deformation of the ZnSe samples resulted in hysteresis loops during four repeated unloading/reloading cycles; in particular, it led to larger deviations in the plots of the penetration depth with respect to the indentation load. Slip enhancement, which may contribute to the "pop-in" observed during unloading and reloading, is one of the mechanisms occurring due to the plastic deformation of ZnSe. The nanoindentation-induced deformations act as non-radiative recombination centers, as confirmed by the reduction in intensity of the CL emission and the CL mapping images. Cross-sectional TEM images revealed that the prime deformation mechanism in ZnSe is slip nucleation on both the basal and pyramidal planes; it appears to be a significant component of contact-induced damage of ZnSe samples.

Acknowledgment

This study was supported by the National Nano Device Laboratories in Taiwan (Contracts NDL98-C03SP-127 and NDL98-C03SP-128). The author thanks Professor Wu-Ching Chou for assistance with the sample preparation and helpful discussions.

References

[1] Mokili B, Charreire Y, Cortes R, Lincot D. Extended X-ray absorption fine structure studies of zinc hydroxo-sulphide thin films chemically deposited from aqueous solution. Thin Solid Films 1996;288:21–8.
[2] Abe T, Ishikura H, Fukuda N, Aung ZM, Adachi M, Kasada H, et al. Demonstration of blue-ultraviolet avalanche photo-diodes of II–VI wide bandgap compounds grown by MBE. J Cryst Growth 2000;214–5:1134–7.
[3] Gerhard A, Nürnberger J, Schüll K, Hock V, Schumacher C, Ehinger M, et al. ZnSe-based MBE-grown photodiodes. J Cryst Growth 1998;184–5:1319–23.
[4] Ishikura H, Fukuda N, Itoi M, Yasumoto K, Abe T, Kasada H, et al. High quantum efficiency blue-ultraviolet ZnSe pin photodiode grown by MBE. J Cryst Growth 2000;214–5:1130–3.
[5] Sato K, Hanafusa M, Noda A, Arakawa A, Uchida M, Asahi T, et al. ZnTe pure green light-emitting diodes fabricated by thermal diffusion. J Cryst Growth 2000;214–5:1080–4.
[6] Lai LS, Sou IK, Law CWY, Wong KS, Yang Z, Wong GKL. ZnSSe-based ultra-violet photodiodes with extremely high detectivity. Opt Mater 2003;23:21–6.
[7] Gaysinskiy V, Singh B, Ovechkina L, Miller S, Thacker S, Nagarkar V. Luminescence properties and morphology of ZnSe: Te films. IEEE Trans Nucl Sci 2008;55:1556–60.
[8] Grillo SE, Ducarroir M, Nadal M, Tournié E, Faurie J-P. Nanoindentation of Si, GaP, GaAs and ZnSe single crystals. J Phys D: Appl Phys 2003;36:L5–9.
[9] Zarudi I, Zou J, Zhang LC. Microstructures of phases in indented silicon: a high resolution characterization. Appl Phys Lett 2003;82:874–6.
[10] Taylor CR, Stach EA, Salamo G, Malshe AP. Nanoscale dislocation patterning by ultralow load indentation. Appl Phys Lett 2005;87:0731081–3.
[11] Haberl B, Bradby JE, Ruffell S, Willams JS, Munroe P. Phase transformations induced by spherical indentation in ion-implanted amorphous silicon. J Appl Phys 2006;100:0135201–9.
[12] Basu S, Barsoum MW, Williams AD, Moustakas TD. Spherical nanoindentation and deformation mechanisms in freestanding GaN films. J Appl Phys 2007;101:0835221–7.
[13] Wen H, Wang X, Li L. Mechanical properties of sol–gel derived $BiScO_3$–$PbTiO_3$ thin films by nanoindentation. J Appl Phys 2006;100:0843151–5.
[14] Fernández P, Piqueras J, Urbieta A, Rebane YT, Shreter Y. Deformation-induced defect levels in ZnSe crystals. Semicond Sci Technol 1999;14:430–4.
[15] Grillo SE, Ducarroir M, Nadal M, Tournié E, Faurie J-P. Nanoindentation study of Zn1−xBexSe heteroepitaxial layers. J Phys D: Appl Phys 2002;35:3015–20.
[16] Triboulet R, Ndap JO, Tromson-Carli A, Lemasson P, Morhain C, Neu G. Growth by solid phase recrystallization and assessment of large ZnSe crystals of high purity and structural perfection. J Cryst Growth 1996;159:156–60.
[17] Oliver WC, Pharr GM. An improved technique for determining hardness and elastic modulus using load and displacement sensing indentation experiments. J Mater Res 1992;7:1564–83.
[18] Chien CH, Jian SR, Wang CT, Juang JY, Huang JC, Lai YS. Cross-sectional transmission electron microscopy observations on the Berkovich indentation-induced deformation microstructures in GaN thin films. J Phys D: Appl Phys 2007;40:3985–90.
[19] Jian SR. Berkovich indentation-induced deformation behaviors of GaN thin films observed using cathodoluminescence and cross-sectional transmission electron microscopy. Appl Surf Sci 2008;254:6749–53.
[20] Kucheyev SO, Bradby JE, Williams JS, Jagadish C, Toth M, Phillips MR, et al. Nanoindentation of epitaxial GaN films. Appl Phys Lett 2000;77:3373–5.
[21] Kucheyev SO, Bradby JE, Williams JS, Jagadish C, Swain MV. Mechanical deformation of single-crystal ZnO. Appl Phys Lett 2002;80:956–8.
[22] Bradby JE, Kucheyev SO, Williams JS, Wong-Leung J, Swain MV, Munroe P, et al. Indentation-induced damage in GaN epilayers. Appl Phys Lett 2002;80:383–5.
[23] Bradby JE, Williams JS, Wong-Leung J, Swain MV, Munroe P. Mechanical deformation of InP and GaAs by spherical indentation. Appl Phys Lett 2001;78:3235–7.
[24] Bahr DF, Kramer DE, Gerberich WW. Non-linear deformation mechanisms during nanoindentation. Acta Mater 1998;46:3605–17.
[25] Wolf B, Belger A, Meyer DC, Paufler P. On the impact of light on nanoindentations in ZnSe. Phys State Solid (a) 2001;187:415–26.
[26] He BC, Cheng CH, Wen HC, Lai YS, Yang PF, Lin MH, et al. Evaluation of the nanoindentation behaviors of SiGe epitaxial layer on Si substrate. Microelectron Reliab 2010;50:63–9.
[27] Coleman VA, Bradby JE, Jagadish C, Phillips MR. Observation of enhanced defect emission and excitonic quenching from spherically indented ZnO. Appl Phys Lett 2006;89:0821021–23.
[28] Bradby JE, Kucheyev SO, Williams JS, Jagadish C, Swain MV, Munroe P, et al. Contact-induced defect propagation in ZnO. Appl Phys Lett 2002;80:4537–9.
[29] Nazarov MV. Cathodoluminescence defectoscopy of ZnS and ZnSe crystals. Mater Sci Eng 2002;B91–2:349–52.
[30] Osipyan YA, Petrenko VF, Zaretskij AV, Whitworth RW. Properties of II–VI semiconductors associated with moving dislocations. Adv Phys 1986;35:115–88.
[31] J-il Jang, Lance MJ, Wen S, Tsui TY, Pharr GM. Indentation-induced phase transformations in silicon: influences of load rate and indenter angle on the transformation behavior. Acta Mater 2005;53:1759–70.
[32] Ruffell S, Bradby JE, Fujisawa N, Williams JS. Identification of nanoindentation-induced phase changes in silicon by in situ electrical characterization. J Appl Phys 2007;101:083531–7.
[33] Kucheyev SO, Bradby JE, Williams JS, Jagadish C, Swain MV, Li G. Deformation behavior of ion-beam-modified GaN. Appl Phys Lett 2001;78:156–8.
[34] Zaldívary MH, Fernández P, Piqueras J. Influence of deformation on the luminescence of GaN epitaxial films. Semicond Sci Technol 1998;13:900–5.